

## Article

# Optimization of the Aircraft Air/Oil Separator by the Response Surface Determined from Modeling of Three-Dimensional Two-Phase Flow

Tomasz Szwarc <sup>1,2</sup>, Włodzimierz Wróblewski <sup>1,\*</sup>  and Tomasz Borzęcki <sup>2</sup>

<sup>1</sup> Department of Power Engineering and Turbomachinery, Silesian University of Technology, 44-100 Gliwice, Poland

<sup>2</sup> Avio Polska sp. z o.o., Advanced Technology Operations, 43-300 Bielsko-Biała, Poland

\* Correspondence: wlodzimierz.wroblewski@polsl.pl

**Abstract:** This paper presents optimisation of the geometry of the aircraft air–oil separator (AAOS) performed to improve the device performance. For this separator type, the most important operating parameters are the oil quality, efficiency and pressure drop. In order to understand the relationships between geometric parameters and their impact on the parameters of the separator operation, an analysis was conducted using the Response Surface Method (RSM). The analysis was made based on the results of numerical simulations and using the volume-of-fluid (VOF) method. Pareto analysis was also carried out, which determined the impact of the inlet width and height and the separator diameter on the device performance. By solving the optimisation task using a genetic algorithm, it was possible to propose a new geometry for the AAOS. The favourable geometric relations for the AAOS are indicated and they are compared with those preferred for other geometries of cyclone separators.

**Keywords:** air–oil separator; cyclone separator; multi-objective optimisation; response surface; DOE; volume-of-fluid method



**Citation:** Szwarc, T.; Wróblewski, W.; Borzęcki, T. Optimization of the Aircraft Air/Oil Separator by the Response Surface Determined from Modeling of Three-Dimensional Two-Phase Flow. *Energies* **2022**, *15*, 7273. <https://doi.org/10.3390/en15197273>

Academic Editor: Chris Bingham

Received: 1 September 2022

Accepted: 28 September 2022

Published: 3 October 2022

**Publisher's Note:** MDPI stays neutral with regard to jurisdictional claims in published maps and institutional affiliations.



**Copyright:** © 2022 by the authors. Licensee MDPI, Basel, Switzerland. This article is an open access article distributed under the terms and conditions of the Creative Commons Attribution (CC BY) license (<https://creativecommons.org/licenses/by/4.0/>).

## 1. Introduction

Cyclone separators are one of the most common separation devices used in various industries. The principle of their operation consists in using a centrifugal force to separate fractions of the introduced mixture. Three types of separation can be distinguished: solid particles from a liquid, liquid from gas or gas from liquid. The main advantages of these devices are compactness and simplicity of design, which result in a low construction cost. Another advantage of cyclones is that they can be used in a wide range of operating conditions. A standard cyclone is made of the inlet part, the cylindrical part and the conical part. The structure of the main geometric parameters are: the inlet dimensions (for a rectangular inlet: height  $a$  and width  $b$ ), the cylindrical part—diameter  $D$ , the cylindrical part—height  $h$ , the cyclone—total height  $H_t$ , the cone—outlet diameter  $B_c$ , the vortex finder—diameter  $D_x$  and length  $S$  (Figure 1A). This is the most common geometry for the separation of solid particles from a gas or liquid. For most standard cyclones and hydrocyclones, these are the characteristic dimensions that make it possible to determine their efficiency and the pressure drop using empirical models developed based on empirical testing results [1–7]. Adequate selection of geometric quantities can improve the separator performance. Analysing to-date reports on the aircraft air–oil separator [8–11], it was found that its geometry (Figure 1B) was not much different from the standard cyclone used for the removal of particulates from gases, and the separation phenomenon was similar to that occurring in gas–liquid cylindrical cyclone (GLCC) separators (Figure 1C) used in the petrochemical industry. This particular type is most often used to separate gas from a liquid or to separate one liquid from another. In order to compare the AAOS geometry with other types of cyclone separators, their basic geometric dimensions are listed in Table 1

compared to the diameter of each separator type. The values of the AAOS ratios for the inlet channel dimensions  $a/D$  and  $b/D$  and the vortex finder diameter  $D_x/D$  are not significantly different from those which demonstrated high separation efficiency in the testing performed by Stairmand [12]. The difference in the  $H_t/D$  ratio is the effect of the fact that the analysed AAOS does not have a conical part. There is no conical part in the GLCC design, so  $H_t = h$  and the difference in the  $h/D$  ratio is 2–14× bigger due to the different use and different operating conditions. There is no vortex finder, either, which means that  $D_x = D$ . As shown in [13–16], changes in the ratios between these parameters may have a substantial impact on the flow field, and consequently on the separator operation efficiency.

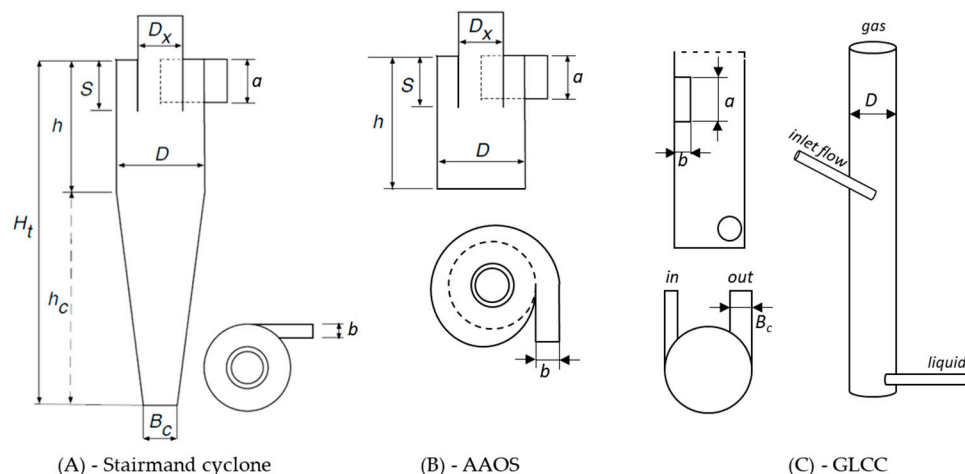


**Figure 1.** Cyclone separator configurations—main dimensions.

**Table 1.** Separator geometric ratios.

	$a/D$	$b/D$	$D_x/D$	$H_t/D$	$h/D$	$S/D$	$B_c/D$
Stairmand [17]	0.5	0.2	0.5	4	1.5	0.5	0.38
AAOS [11]	0.46	0.28	0.39	1.05	0.52	1.0	
GLCC Minh [18]	0.5	0.5	0.5		18.1	1	0.9
GLCC Farchi [19]	0.5	0.1	1.0	2.5		1	0.2
GLCC Erdal [20]	0.4	0.4	1.0	16.5		1	0.6

Zhu [13] performed experimental testing of cyclones with small dimensions operating at a high flow rate. The separator had a constant diameter and the testing concerned the impact of  $h$ ,  $D_x$ ,  $S$  on the efficiency of the separation of particles and on the pressure drop. It was found that  $(h - S)$  affected the separation characteristic substantially. The pressure drop decreased significantly when height  $h$  increased, or when the vortex finder length  $S$  got smaller. The geometry with the ratios of  $h/D$  and  $S/D$  was tested in the range of 0.75 – 4.5 and 0.5 – 1.5, respectively, and the optimal efficiency was obtained for the ratios of  $h/D = 2$  and  $S/D = 1$ .

Brar [21] investigated the impact of the Stairmand separator diameter  $D$  using CFD tools. Calculations were performed for diameters  $0.8D$ ,  $D$ ,  $1.2D$ , determining the efficiency of the separation of particles and the pressure drop of the separator. A change in diameter  $D$  involved a change in the pressure drop value: for  $0.8D$  a drop by 4.15% and for  $1.2D$  a rise by 16.2% compared to a separator with diameter  $D$ . The separation efficiency decreased by 3.3% for diameter  $0.8D$  and rose by 3.9% for diameter  $1.2D$ .

Tauber [8] conducted experimental research on the AAOS connected to the diagnostics system of a turbo-propeller engine. The tests were conducted for a wide range of operating conditions, taking account of changes in the oil amount, temperature and the volume fraction of air delivered to the separator. The impact of  $D_x$  was investigated and

it was found that a rise in its value involved a rise in the oil quality and a drop in the separation efficiency.

Furino [10] performed CFD calculations examining the impact of geometric parameters on AAOS efficiency. Two configurations were tested: the AAOS (Figure 1B), changing parameters  $(a, b, D, h, D_x, S)$ , and the geometry presented in Figure 1A, changing the shape of the outlet orifice and, thereby, the outlet orifice surface area. The results of the calculations show that changes in  $D_x$  and  $S$  do not cause a significant change in the separation efficiency. It was found that a 30% reduction in the inlet surface area (parameters  $a, b$ ) affects the separation efficiency to a degree similar to that caused by the same reduction in  $D$ . The testing was limited due to the small number of AAOS configurations; no impact was mentioned of geometry on the pressure drop and no testing was performed on the impact of geometric parameters on  $OQ$ .

Elsayed carried out research aiming to improve the Stairmand separator geometry using mathematical models and CFD tools [14,22,23]. The testing of parameters  $a, b, D_x, h$  and  $S$  made it possible to determine their impact on the pressure drop and the separation efficiency. It was shown that the maximum tangential velocity in the separator decreased with a rise both in  $a$  and  $b$ . The observed change in the inlet dimensions did not cause a significant difference in either static pressure or axial velocity values. The testing results indicate that the optimal value of the  $b/a$  ratio should be included within the range of  $0.5 - 0.7$ . A significant decrease in the pressure drop was observed for the interval of  $0.25 \leq a/D \leq 0.4$  and when  $a/D \geq 0.4$ . The optimal ratio of  $b/D = 0.236$  was found, and designs with a wide inlet, where the  $b/D$  ratio is higher than the distance between the cylindrical part and the vortex finder wall, were not recommended. A rise in  $D_x$  involved a decrease in the maximum tangential velocity in the cyclone. The separation efficiency was not significantly affected above the ratio of  $h/D = 1.8$ . The impact of the change in the height of the separator cylindrical part  $h$  on efficiency and the flow field was less important compared to the effect of changes in the cone height  $h_c$ . The maximum tangential velocity in the cyclone decreased with a rise in height  $h$  and  $h_c$ . Changes in these parameters had no effect on the maximum tangential velocity in the separator cylindrical part, either. An increase in length  $S$  involved a slight change in the distributions of static pressure and axial and tangential velocities. Further studies conducted by Elsayed [17,23,24] enabled a more effective selection of geometric parameters to achieve the separator optimal operation. The first attempts at optimisation [23] for 7 parameters  $(a, b, h, H_t, D_x, S, B_c)$  focused on minimizing the pressure drop using the RSM analysis based on the Muschelknautz mathematical model and a CFD model. The design of the experiment was chosen according to the Box–Behnken method. The RSM goodness-of-fit function was a second-order polynomial, and the optimisation was carried out using the Nelder–Mead (NM) method (a.k.a. the downhill simplex method). The CFD results for the new geometry showed a pressure drop by more than a half lower compared to the geometry analysed by Stairmand at identical parameters of operation. Further studies [17] focused on multi-objective optimisation using a model of neural networks. The obtained results were verified by means of simulations based on a CFD model. The geometric parameters were selected as in [23], and the minimal pressure drop and efficiency maximisation were established as the objective functions. The RSM analysis was carried out using a second-order polynomial, and the multi-objective optimisation process was run using a genetic algorithm. Multi-objective optimisation was also performed during the studies described in [24], using the same objective functions but four parameters  $(a, b, D_x, S)$ . A CFD model and a neural network model were used for the testing and a genetic algorithm was applied for the optimisation process. Comparing the results from previous testing [23], the NM method was found to have a downside because the result can depend on the initial condition, which leads to the achievement of a local minimum. The CFD analysis results confirmed an improvement in the performance of the optimised cyclone.

Singh [25] proposed a new approach coupling three surrogate models (kriging, radial basis functions and support vector regression) with efficient multi-objective optimisation

(EMO). The algorithm was used to optimise a cyclone geometry described by seven design variables ( $a, b, h, H_t, D_x, S, B_c$ ). NSGA-II genetic algorithm calculations were performed for comparison. The results indicate that the Pareto set designs found using EMO outperform the designs found by means of the NSGA-II, using significantly fewer function evaluations. The new method made it possible to shorten the computation time.

Sun tested a gas cyclone investigating the impact of geometric parameters on the pressure drop and the separation efficiency [26]; the cyclone geometry was also optimised [27]. The testing was based on the RSM using the central composite design (CCD) and CFD model calculations. The Stairmand geometry of the separator was applied to study the parameters [26]. The results of the Pareto analysis point to a substantial impact of parameters  $D_x, b, a$  on the pressure drop and a significant effect of  $a, H_t, b, D_x$  on the separation efficiency (the quantities are mentioned in the order from the biggest to the smallest effect). The optimal solution was obtained for the following ratios:  $a/D = 0.56, b/D = 0.2, h/D = 1, D_x/D = 0.451, S/D = 0.2$ . The geometry optimisation from [26] was performed using a genetic algorithm. In order to reduce the number of optimised parameters, a screening experiment was conducted for  $a, b, h, D_x, S, B_c$  and for surface roughness  $e$ , which made it possible to identify the parameters that were statistically significant. For the pressure drop,  $b, D_x$  were significant, while  $b, D_x, a, e$  were significant for the separation efficiency.

Earlier research on separators was overwhelmingly concerned with industrial separators, which, considering their varied applications, were characterized by different geometries. Due to size limitations, the investigated AAOS had no conical part. For the AAOS under analysis, the literature survey failed to reveal a study that could be used for comparison with the current research. In most cases, the separation process was accompanied by other phenomena due to the type of the applied mixture. In addition, it should be mentioned that it is very difficult to find studies that enable precise determination of the size and distribution of air bubbles. The separation phenomenon in the AAOS is based on the separation of air bubbles appearing in the oil due to the lubrication of various components in the engine [11]. Models used for separators of solid particles cannot be used in such a situation due to ongoing changes in the geometric parameters of air bubbles in the process of coalescence and decomposition.

This paper presents the process of the AAOS geometry optimisation for operating conditions that typically occur during an aircraft take-off. The key geometric parameters affecting the performance of the considered aircraft separator were selected. The testing was performed at the geometric constraints due to the oil tank structure and the correct location of the AAOS relative to the oil level in the tank. Parameters  $a, b, D$  were chosen for the optimisation. The separator numerical simulations were performed for the adopted design of experiment using the two-phase VOF model with the RNG  $k - \epsilon$  turbulence model. Based on the results, the RSM was created using a non-parametric regression algorithm, and a Pareto analysis was conducted. The analysis determined the effect of geometric dimensions on the AAOS performance. Multi-objective optimisation was performed to find geometries with better-operating parameters for the adopted boundary conditions, taking the minimum pressure drop, the maximum efficiency and  $OQ$  as the objective function.

## 2. Numerical Model

### 2.1. Mathematical Model

The two-phase flow was modelled using the volume-of-fluid method [28]. The model type was chosen due to the possibility of creating a free surface between air and oil. This is an important feature considering the oil tank included in the simulation. The free surface will make it possible to determine the oil level in the tank and its influence on the separator operation. The continuity equation is solved:

$$\frac{\partial}{\partial t}(\rho) + \nabla \cdot (\rho \vec{v}) = 0 \quad (1)$$

where  $\rho$  is the mixture density calculated from:

$$\rho = \alpha_a \rho_a + (1 - \alpha_a) \rho_o \quad (2)$$

where  $\rho_a, \rho_o$  are densities of air and oil, respectively, and  $\alpha_a$  is the volume fraction of air which is, in this case, the second phase.

$$\frac{\partial}{\partial t} (\alpha_a \rho_a) + \nabla \cdot (\alpha_a \rho_a \vec{v}_a) = 0 \quad (3)$$

The volume fraction equation is not solved for the oil phase (primary), and the oil-phase volume fraction is computed based on the following constraint:

$$\alpha_a + \alpha_o = 1 \quad (4)$$

For this case, the volume fraction equation is solved through an implicit formula. A single momentum equation is solved throughout the domain, and the resulting velocity field is shared among the phases. The momentum equation, shown below, is dependent on the volume fractions of all phases through quantities  $\rho$  and  $\mu$ .

$$\frac{\partial}{\partial t} (\rho \vec{v}) + \nabla \cdot (\rho \vec{v} \vec{v}) = -\nabla p + \nabla \cdot [\mu_{eff} (\nabla \vec{v} + \nabla \vec{v}^T)] + \rho \vec{g} + \vec{F} \quad (5)$$

Turbulence was simulated using the RNG  $k - \varepsilon$  model [29]. The equations for turbulence kinetic energy  $k$  and the dissipation rate of turbulent kinetic energy  $\varepsilon$  are solved:

$$\frac{\partial}{\partial t} (\rho k) + \frac{\partial}{\partial x_i} (\rho k v_i) = \frac{\partial}{\partial x_j} \left( \alpha_k \mu_{eff} \frac{\partial k}{\partial x_j} \right) + G_k - \rho \quad (6)$$

$$\frac{\partial}{\partial t} (\rho \varepsilon) + \frac{\partial}{\partial x_i} (\rho \varepsilon v_i) = \frac{\partial}{\partial x_j} \left( \alpha_\varepsilon \mu_{eff} \frac{\partial \varepsilon}{\partial x_j} \right) + C_{1\varepsilon} \frac{\varepsilon}{k} G_k - C_{2\varepsilon} \rho \frac{\varepsilon^2}{k} - R_\varepsilon \quad (7)$$

In the above equations,  $\alpha_k$  and  $\alpha_\varepsilon$  are the inversed effective Prandtl numbers for  $k$  and  $\varepsilon$ , respectively.  $C_{1\varepsilon}$  and  $C_{2\varepsilon}$  are constant values of 1.42 and 1.68, respectively. The scale elimination procedure in the RNG theory results in a differential equation for turbulent viscosity. Effective viscosity  $\mu_{eff}$  is expressed as:

$$\mu_{eff} = \rho C_\mu \frac{k^2}{\varepsilon} \quad (8)$$

with  $C_\mu = 0.0845$  derived using the RNG theory. The near-wall modelling was obtained by Enhanced Wall Treatment.

## 2.2. Geometry of the Separator Domain and Boundary Conditions

The computational domain (Figure 2) consisted of the AAOS model (marked in grey) and the auxiliary domain (grey-blue). The top left-hand corner of the figure shows a top view of the fluid domain with two marked planes: 1–1 and 2–2; below is a cross-section of the auxiliary domain with a marked oil outlet. On the right side of the figure, there is a cross-section of the separator with the numerical grid marked in two planes.

The boundary condition at the air/oil inlet was the mass flow rate of air and oil. The air/oil volume flow ratio totalled 2.2. Considering the calculations performed with structure maps and the close distance from the scavenge pump, a uniform phase distribution could be assumed. The separated air flowed through the vortex finder to the air outlet, and the separated oil, to the oil outlet located at the bottom of the auxiliary domain (cf. Figure 2). A boundary condition of static pressure equal to atmospheric pressure was assumed at both outlets. In order to stabilize the flow in the domain, the value of the oil backflow volume fraction was assumed as 0 at the air outlet; 0 was also assumed for the air

fraction at the oil outlet. The turbulent intensity of 5% and a turbulent viscosity ratio of 10 were assumed for the inlet. There was no heat exchange with the environment. The air was treated as a perfect gas. The oil type met the MIL-23699 specifications. The oil properties in the simulation were selected for a specific temperature.

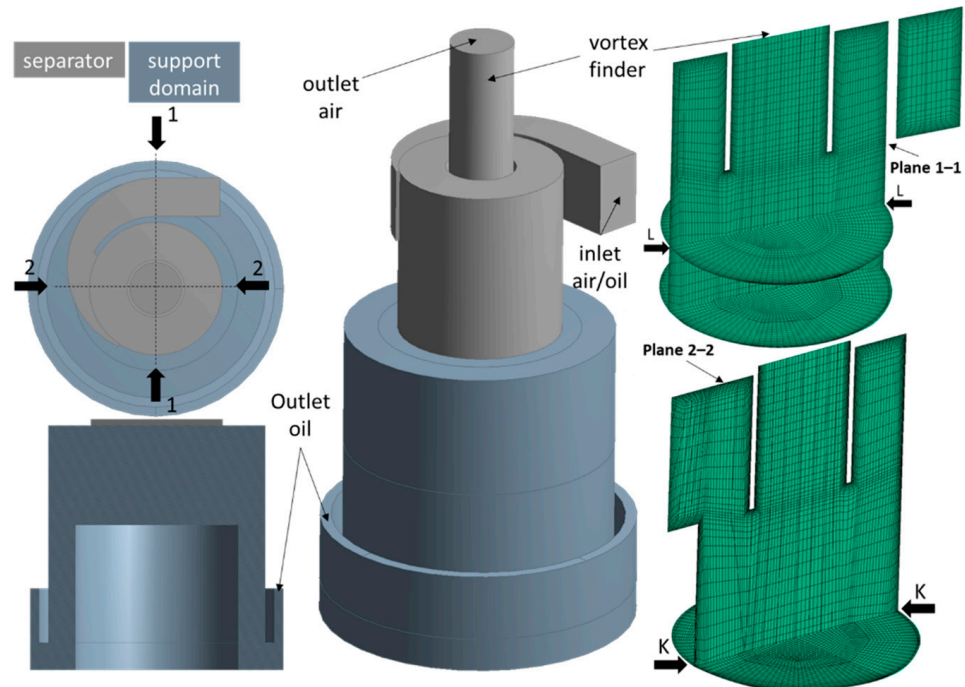


**Figure 2.** Calculation domain and numerical mesh.

The domain was modified to investigate the effect of geometry on performance. Previous research on the separator [11] showed the impact of the oil level on OQ and on efficiency. The oil level was affected by boundary conditions, as well as static pressure at the oil and air outlets. Changes in the separator geometric parameters will involve changes in the pressure drop, which is another variable that causes changes in the oil level in the domain. In order to keep the oil level constant, regardless of the pressure drop, atmospheric pressure was applied at the outlets, and the reference pressure location was selected in the model settings to take account of the effect of hydrostatic pressure in the oil outlet cross-section. The geometric model was parameterized to enable automatic changes in the separator's most important geometric parameters (Table 1, Figure 2).

### 2.3. Selection of the Numerical Mesh

The first stage was to select the numerical mesh discretisation. A study of the solution independence of the computational mesh density was carried out. The geometry of the separator domain was discretised with hexagonal elements.

A transient-type analysis was performed. The VOF model with implicit formulation and enabled implicit body force was applied. The numerical schemes for the current analysis were selected based on the analysis performed in [11]. A coupled scheme was selected as the algorithm for the pressure–velocity coupling. A “no-slip” wall boundary condition was assumed. The time step used in the simulations was related to the global Courant number. A variable time step with the global Courant number of 64 was applied, which corresponded to time steps in the interval of  $1 \times 10^{-4} \div 1 \times 10^{-5}$  s. After the oil level in the domain was stabilised, the computations were continued for more than 10 s to average the results. The selection of the VOF fluid model and the RNG  $k - \epsilon$  turbulence model was based on validation against experimental data presented in [9,11].

The typical parameters used to determine the performance of a GLCC separator are as follows: Liquid Carry Over (LCO), Gas Carry Under (GCU) and pressure drop ( $dP$ ).

The task of multi-objective optimisation is to improve the performance of the gas–liquid separator operation. Parameters LCO, GCU and  $dP$  are in this case the objective functions. In the aircraft separator analysis, it is assumed that the efficiency parameter  $\eta_s$  is defined as the ratio of the difference between the oil volumetric flow at the inlet ( $\dot{V}_{o, inlet}$ ) and the flow leaving the vortex ( $\dot{V}_{o, vortex}$ ) to the oil volumetric flow at the inlet (Equation (9)).

$$\eta_s = \frac{\dot{V}_{o, inlet} - \dot{V}_{o, vortex}}{\dot{V}_{o, inlet}} \quad (9)$$

The GCU quantity for the GLCC separator is replaced by the oil quality (OQ), defined as the ratio of the oil volumetric flow rate at the separator inlet to the sum of the volumetric flow rate of air and oil at the bottom oil outlet:

$$OQ = \frac{\dot{V}_{o, inlet}}{(\dot{V}_{air} + \dot{V}_{oil})_{oil outlet}} \quad (10)$$

The calculations were performed for 5 meshes with the following numbers of elements: 167 k, 374 k, 633 k, 864 k and 1095 k. For others, denser meshes—uniform refinement over the entire domain was assumed. The mesh general quality parameter was in each case higher than 0.4, and the  $y^+$  value totalled  $\sim 30$ . An analysis was made of the impact of the numerical mesh density on OQ, the separation efficiency and the pressure drop (Figure 3). All the presented results were compared to the results obtained on the mesh with 1095k elements. An increase in the number of elements did not significantly affect the separator efficiency. The pressure drop value changed by 1% for the smallest mesh with 167k elements and by 0.5% for the mesh with 374k elements; the other meshes showed no significant differences. The greatest effect of the mesh density was observed for the oil quality (OQ). The meshes with 167k and 374k elements gave values of 17% and 6% lower, respectively. On the mesh with 633k elements, the difference totalled 3%, whereas for the mesh with 864k elements, a 2% difference was observed. Considering the obtained differences in the separator operating parameters, the computation time and the number of cases, the mesh with 633k elements was selected for further analyses. The selected mesh makes it possible to obtain stable results in about 2 weeks on a PC cluster using 14 cores.

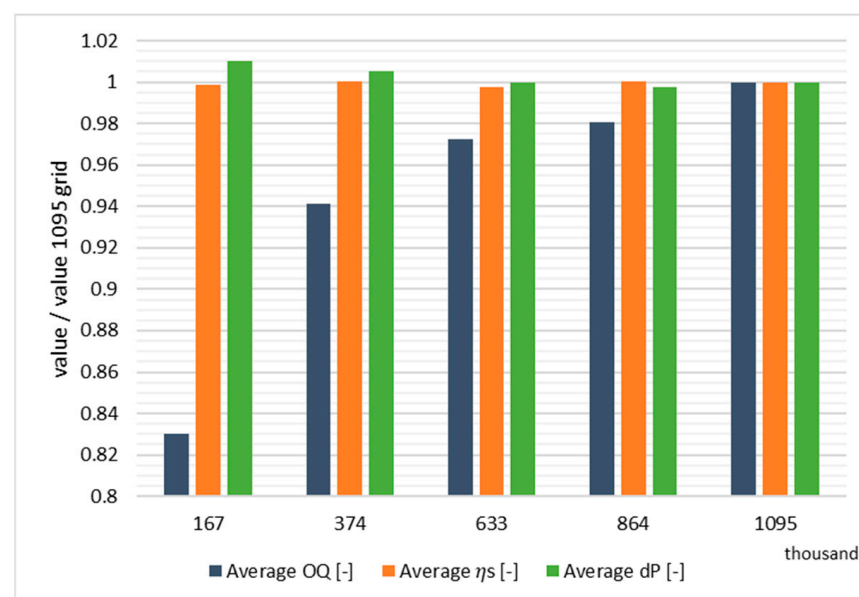
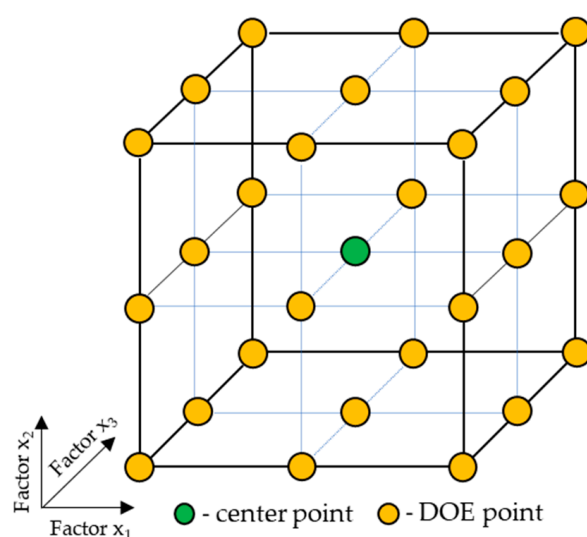


Figure 3. Mesh impact on the analysed parameters (reference value for 1095k mesh).

### 3. Design of the Experiment Selection and the Optimisation Algorithm

The standard approach in optimisation is to check the influence of one parameter, keeping the others constant, until optimal performance for operating conditions is found. The analysis of a single parameter is often time-consuming and may fail to detect possible interactions between other parameters. One of the popular methods for finding relations between parameters is DOE. The choice of the design of the experiment (DOE) depends on its objectives and the number of parameters to be investigated. In order to get the response and interactions of any combination of parameters, a multivariate parametric study was conducted. Before the analysis can be performed, the DOE has to be selected from a number of proposals. A method based on the RSM, popular in solving engineering problems, was used for this purpose. In the case of the RSM, it is good for the DOE to have the right features, such as satisfactory distribution across the entire design space and rotability [30]. The most common are: the central composite circumscribed (CCC) design, the central composite inscribed (CCI) design, the central composite face-centred (CCF) design, the full factorial array 3 level, the Box–Behnken design and the orthogonal array. The main factor affecting the choice of the DOE was to find a configuration that would reduce the number of computational cases, providing at the same time the opportunity to describe the separator behaviour in the entire available design space. The DOE should provide the most information about the output quantities and ensure the lowest possible uncertainty of the prediction of their future values. Assuming a nonlinear relationship, at least 3 levels are required for each factor. The CCI and the CCC design were rejected because of the large number of points due to the occurrence of 5 levels for each factor. For the CCC design, some calculation points would be outside the assumed design space. The CCF design is poor at a precise estimation of coefficients and is not rotatable. The Box–Behnken method and the orthogonal array have combinations of points within the design space, but they lack points in the corners, which may be important due to the uncertainty of values predicted within the selected range of geometric dimensions. Therefore, the selected DOE is the Full Factorial Array 3 Level (Figure 4). Although it is not rotatable, it has evenly distributed points throughout the entire design space, has points occurring in the corners and is symmetrical. This DOE type is not often used because its computational cost increases significantly with a rise in the number of parameters. However, if this number is kept low, the design becomes acceptable.



**Figure 4.** Graphical view for the three-level full factorial array ( $3^3$ ).

In order to select a suitable RSM, three types of surface fitting were considered: kriging, genetic aggregation and non-parametric regression. Kriging is a method in which interpolation occurs exactly through points. If a scatter of results occurs, which was the case in the

analyses described herein, the method was used only to make a preliminary assessment of the surface course in relation to the other types of the RSM. Genetic aggregation is a versatile, efficient and reliable procedure that makes use of a genetic algorithm to generate populations of different response surfaces solved in parallel. The algorithm automates the process of selecting, configuring and generating the type of the response surface best fitting each output parameter. Using the various available response surface types (the second-order polynomial, non-parametric regression, kriging and the moving least squares method), genetic aggregation automatically creates the response surface type that is the most appropriate approach for each outcome. Non-parametric regression belongs to the group of support-vector methods (SVMs). It is often used in cases involving a scatter of results. The main principle of this model is to adopt a tolerance value that creates a narrow range between the response values in a given set. The range is created to include most of the set points or the main response points. The created response surface will then be within the margin of the adopted tolerance.

The multi-objective genetic algorithm (MOGA) method was selected to carry out the optimisation process. It is a variant of the non-dominated sorted genetic algorithm-II (NSGA-II). Maximisation of the efficiency and OQ parameters and minimisation of the pressure drop were chosen as the objective functions. The response surface (RS) and the MOGA were built using the DesignXplorer, which described the relationship between the design variables and the performance of the product by using the DOE, in combination with the RS.

## 4. Separator Optimisation

### 4.1. Design of Experiment

The following 3 geometric parameters (factors) were adopted for the analysis:  $a$ ,  $b$  and  $D$ . The applied DOE, for 3 levels, gives  $3^3 = 27$  cases, which is a number acceptable in terms of the computation time. The parameters related to the vortex finder geometry will not be investigated in this case.

The analyses covered two DOEs for different ranges of the inlet cross-section parameters: RS1, with the inlet with the ratio of  $b/a > 1$  and RS2, with the inlet with the ratio of  $b/a < 1$ . Both DOEs use the same diameter values:  $0.9D$ ,  $D$ ,  $1.1D$ . A constant height of the cylindrical part below the inlet was kept ( $h - a$ ). Two ranges of the  $b/a$  ratio were tested due to the limitation of the separator length  $h_{max}$ . The value was selected to meet the  $h < h_{max}$  condition (cf. Table 2).

### 4.2. Response Surface

In order to obtain a better fit of the response surface, calculations were made of additional verification points located in the design space. The points were selected by the program. Calculations were performed on 22 and 15 verification points for RS1 and RS2, respectively. The first design has more verification points because it was necessary to determine from what number of points the relative average absolute error in fitting the DOE and the verification points to the surface (Table 3) stopped decreasing by more than 1%. At genetic aggregation, a very good fit of the surface was found for the separator efficiency parameter (error in the goodness of fit of DOE and verification points, 0%), while for the oil quality, the error was 7 times higher. The error value for the pressure drop was 5 times lower compared to the RS1 verification points. In the case of the RS2, the error was twice smaller for OQ and 1% lower for the pressure drop (cf. Table 3). Because OQ is the factor deciding the correct functioning of the oil system, the non-parametric regression method was selected.



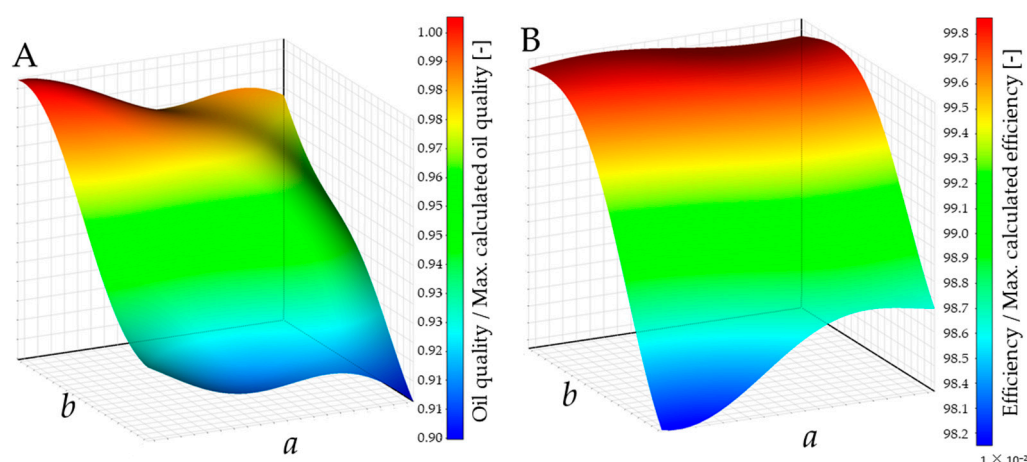


Figure 5. (A) Oil quality response surface; (B) Efficiency response surface.

#### 4.3. Optimization Task

Table 4 compares the geometric parameters of the optimised New AAOS geometry to the reference geometry (Ref. AAOS) and other geometries reported in the literature. Ref AAOS refers to the separator tested on the experimental test bench [9,11]. The  $a/D$  ratio of the new geometry is approx. 30% higher compared to the reference geometry. The obtained  $b/D$  ratio is similar to the Ref. AAOS value, the  $D_x/D$  value increased compared to the reference geometry by 15%, while the  $h/D$  ratio increased by 27%. The obtained dimensional ratios of the New AAOS geometry are not similar to any of the geometries investigated earlier, while the values of the obtained ratios were included within the range presented in Table 4.

Table 4. Comparison of geometric parameters of the current and previous optimal models.

	New AAOS	Ref. AAOS	Stairmand [12]	Sun [27]	Ravi [31]	Elsayed [23]	Elsayed [17]	Elsayed [24]	Elsayed [24]	Sgrott Jr. [32]
$a/D$	0.60	0.46	0.50	0.6	0.40	0.62	0.60	0.26	0.49	0.41
$b/D$	0.29	0.28	0.20	0.2	0.15	0.24	0.20	0.15	0.16	0.50
$D_x/D$	0.45	0.39	0.50	0.5	0.40	0.62	0.55	0.42	0.62	0.50
$h/D$	1.29	1.01	1.50	1.0	1.10	1.62	1.41	1.50	1.50	1.53
$S/D$	0.60	0.52	0.50	0.2	0.40	0.62	0.60	0.50	0.50	0.72

Table 5 compares the results of the operating parameters for 3 geometric configurations of the AAOS: the New AAOS, the Ref. AAOS and the Case15-RS2 (C15RS2) variant, which has the same  $b/a$  ratio for the inlet channel as the Ref. AAOS. The C15RS2 geometry was selected to observe the differences occurring between dimensions  $a, b, D$  (New AAOS vs. C15RS2) and the impact of the inlet-separator inclination compared to a horizontal inlet (Ref. AAOS vs. C15RS2). The New AAOS geometry shows the highest OQ compared to the others (0.26 higher than the Ref. AAOS). The New AAOS efficiency was slightly lower compared to the Ref. AAOS, but relative efficiency higher than 0.995 is accepted as satisfactory. The value of the pressure drop for the New AAOS was 0.31 lower compared to the same efficiency for the Ref. AAOS. The optimised geometry has a higher OQ, acceptable efficiency and a lower pressure drop. It also has a diameter  $D$  reduced by 20% and the total separator length  $h$  bigger by 14% compared to the Ref. AAOS, which was included within the assumed limits.

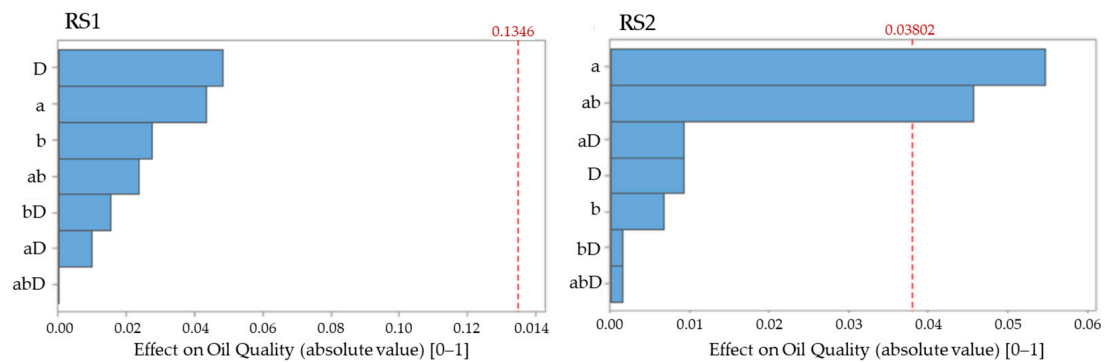
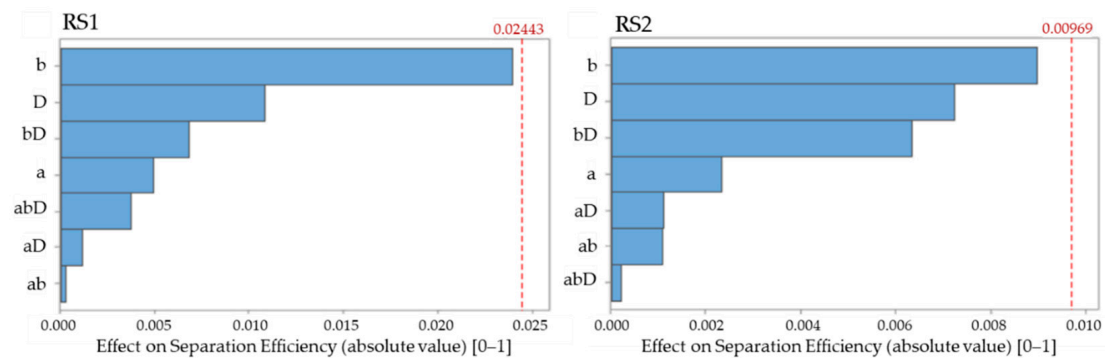
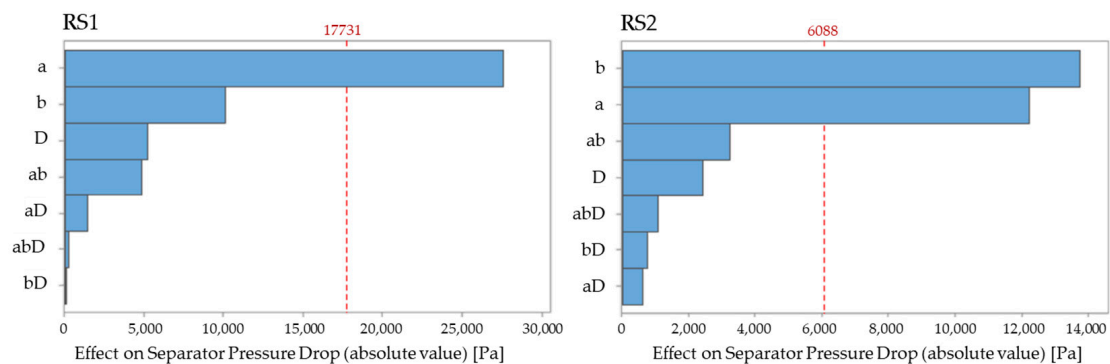
**Table 5.** Comparison results (results/max. value from DOEs).

	Oil Quality/Max. Calculated Oil Quality [-]	Efficiency/Max. Calculated Efficiency [-]	Pressure Drop/Max. Calculated Pressure Drop [-]
New AAOS	0.99	0.997	0.38
C15RS2	0.88	0.998	0.34
Ref. AAOS	0.73	0.999	0.69

## 5. Analysis of Results

### 5.1. Pareto Analysis

A comparative Pareto analysis was conducted for the two variants of the design of the experiment described above: RS1 and RS2. The bars that cross the red dashed line on the Pareto charts in Figures 6–8 show which terms are statistically significant. The red dashed line represents a significance level of 0.05, which indicates a 5% risk of the wrong association between the response and each term.

**Figure 6.** Pareto chart for the oil quality for both DOE variants.**Figure 7.** Pareto chart for the separation efficiency for both DOE variants.**Figure 8.** Pareto chart for the pressure drop for both DOE variants.

The analysis made it possible to observe that there was no significant parameter affecting  $OQ$  for the RS1 variant, while the highest effect was for  $D$  and then for  $a$  and  $b$  with no big difference in the impact of the two parameters (cf. Figure 6-RS1). For RS2, parameter  $a$  and the relationship between  $a$  and  $b$  had a substantial effect on  $OQ$ , the diameter being a less important parameter (Figure 6-RS2).

The results are different when it comes to the separator efficiency. No statistically significant parameters were found. For RS1, parameter  $b$  was the closest to the significant limit, then for  $D$ , the effect was smaller by half (Figure 7). For the RS2 variant, the order of the first four parameters is the same as for RS1. The effect of diameter  $D$  is smaller and there is a correlation between  $b$  and  $D$  compared to  $b$  in the RS1 variant (Figure 7).

In the case of the pressure drop, parameter  $a$  is significant for RS1, whereas the other parameters ( $b$  and  $D$ ) are not. For the RS2 variant, both  $b$  and  $a$  are significant parameters (Figure 8).

It was found that the range of the inlet ratios ( $b/a > 1$  vs.  $b/a < 1$ ) had an impact on which parameters would be significant. The effect of geometric parameters on  $OQ$  will depend on the range of the inlet dimensions. In the first range, no parameters were found with a significant impact on the improvement in  $OQ$ , whereas the second pointed to height  $a$  and the  $ab$  correlations. In terms of the separator efficiency, the range had no influence on the appearance of statistically significant parameters. It was only found that a change in the effect of dimensions  $b$  and  $D$  was stronger for the second range. For the pressure drop, like in the case of the oil quality, an impact was observed of the range of the inlet dimensions on changes in statistically significant parameters. When  $b/a > 1$ , the only significant parameter was height  $a$ . For  $b/a < 1$ , on the other hand, the significant parameters were width  $b$  and height  $a$ .

### 5.2. The Effect of Geometric Parameters on the Separator Operation

The testing covered the impact of the correlations between the AAOS geometric parameters  $b/a$  and  $h/D$  on efficiency,  $OQ$  and the pressure drop. The analysis below includes all available results of the calculations from the prepared DOEs together with their RS verification points. The obtained efficiency values were compared with the results of the testing carried out for the reference geometry [10].

The trend is similar to the results obtained by Furino [10]. The model indicated the separator relative efficiency lower by about 0.18 for  $b/a = 0.4$ . The remaining values are within the range of the results of the present study (cf. Figure 9A). It was found that at a ratio of  $b/a > 1$ , there was a drop in efficiency below the value of 0.99. Figure 9B shows the dependence of the separator efficiency on the  $h/D$  ratio. The highest efficiency values were obtained for  $b/a > 1.5$  and for  $0.95 < h/D < 1.1$ . It was noticed that for a constant value of  $b/a$ , the efficiency decreased with a rise in  $h/D$ . Using dimensions that meet the conditions of  $b/a$  around 0.5 and  $h/D$  around 1, it is possible to obtain a separator with the highest efficiency without losing the design compactness.

Figure 10 shows the effect of geometric parameters on the  $OQ$  relative value. For the analysed changes in the separator geometry, a decrease was observed in relative  $OQ$  of about 0.15 when  $b/a > 1$ . For  $b/a < 0.5$ , the  $OQ$  highest relative value of more than 0.95 was observed (Figure 10A). Analysing the impact of  $h/D$ , it was noticed that  $OQ$  improved with an increase in the  $h/D$  ratio, and above the value of 1.2, it exceeded 0.9. For  $h/D > 0.99$  and  $b/a < 1$ , the recorded oil quality values exceed 0.85 (Figure 10B).

Analysing the pressure drop for the AAOS (Figure 11), two high values of the parameter were found in the entire range under consideration. The relative pressure drop reached as much as about 0.74 for  $b/a = 0.58$ , and the maximum value for  $b/a = 1.73$  (Figure 11A). The smallest relative pressure drop occurred for  $b/a = 0.69$  at  $h/D = 1.2$ . For constant values of the  $b/a$  ratio, the pressure rises with a rise in the value of  $h/D$ . For the range of  $b/a > 1.56$ , the relative pressure drop value varied by about 0.1 and below the change, totalled about 0.05–0.07 (Figure 11B).

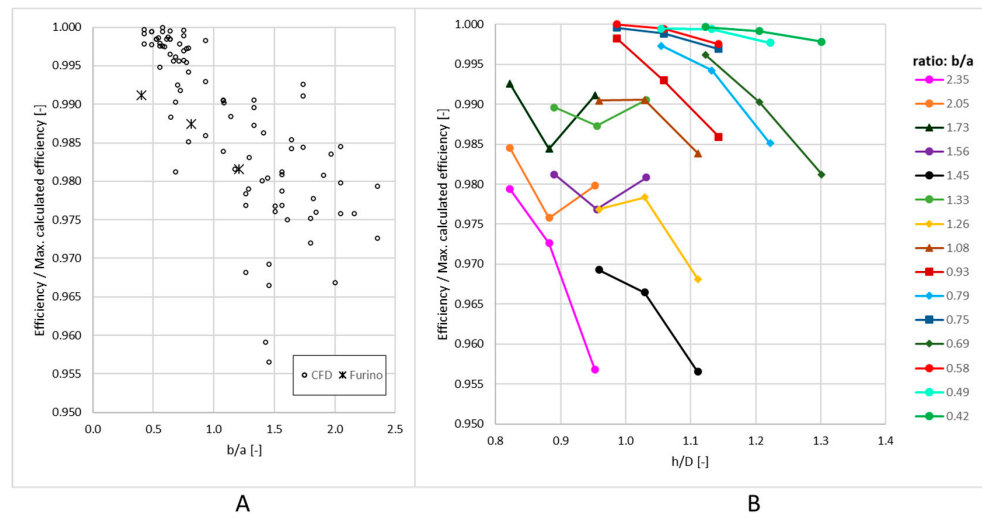


Figure 9. (A)  $b/a$  ratio impact on efficiency; (B)  $h/D$  ratio impact on efficiency.

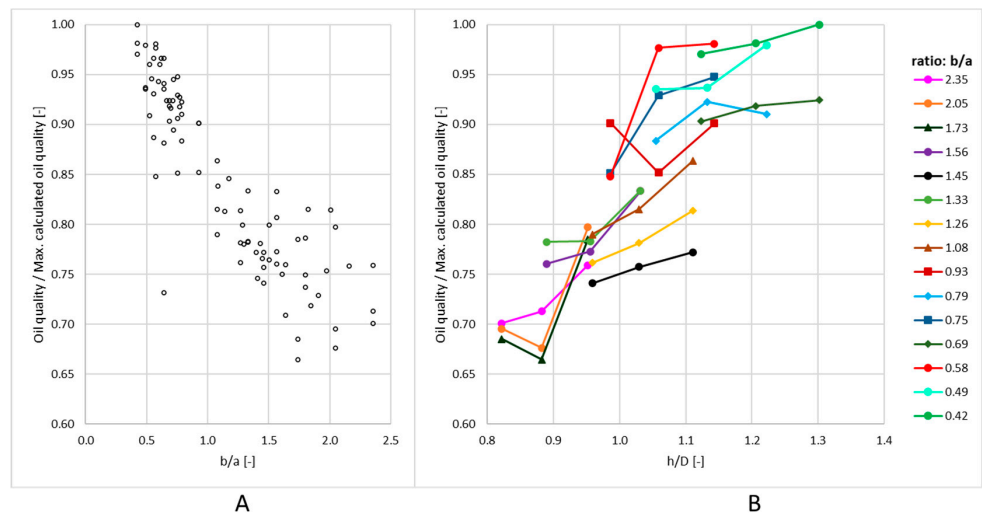


Figure 10. (A)  $b/a$  ratio impact on the oil quality; (B)  $h/D$  ratio impact on the oil quality.

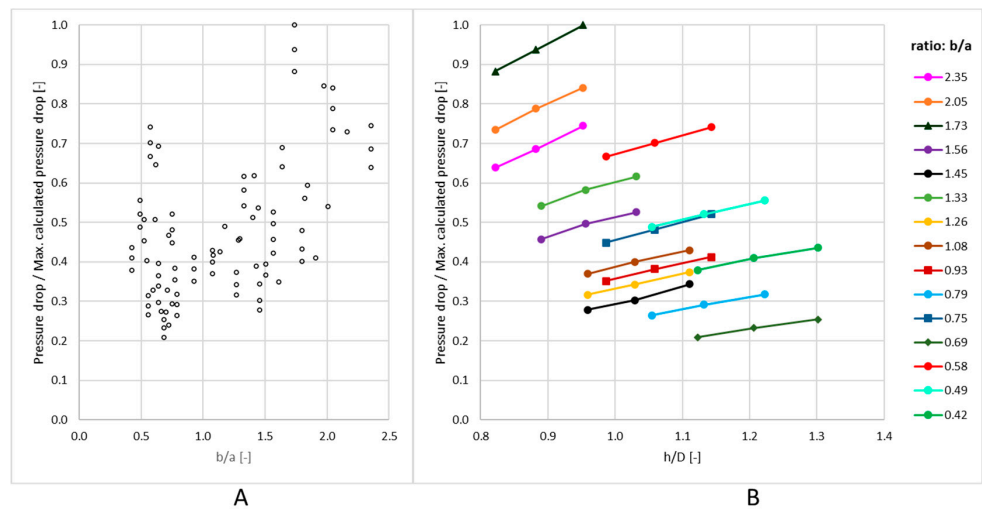


Figure 11. (A) Pressure drop vs.  $b/a$  ratio; (B) Pressure drop vs. the  $h/D$  ratio.

From the presented numerical testing of the aircraft separator carried out at the set boundary conditions, it follows that:

- The highest efficiencies are obtained for  $b/a < 1$  and  $h/D > 0.95$
- The highest oil quality values are obtained for geometry with  $b/a < 0.6$  and  $h/D > 1.05$
- An increase of  $b/a$  and decrease of  $h/D$  ratios involves a higher pressure drop.

### 5.3. Comparison of Flow Field Structures for Different Configurations of the Separator

#### 5.3.1. Oil Fraction Contours

The flow structures are compared for the configurations in Table 5. The plane in Figure 12 is located on plane 1–1 (Figure 2), while the plane in Figure 13 is perpendicular to plane 1-1 and is located at a height  $0.25b$  from the bottom edge of the inlet. It follows from the simulations of various AAOS configurations that the oil-phase concentration locations are similar for all geometries. Separated oil concentrates in the top part of the separator and, making a full turn in it, is directed back to the inlet space, where it mixes with a fresh inflowing mixture (Figures 13 and 14). This phenomenon is unfavourable due to the re-mixing of oil. It appeared also at other boundary conditions [9,11]. On the left edge of the cross-section, above the vortex finder, is the region where the two streams of the mixtures are joined. For each configuration, a space was found between the streams where no oil fraction occurred (Figure 13). In the New AAOS and the C15RS2 configuration, at the cylindrical part inlet, oil concentrates in alternating layers with higher and lower oil content. For the Ref. AAOS configuration, the formation of a film with an increasing concentration of oil can be observed as the distance to the wall gets shorter. Figure 12 shows an even distribution of the oil film on the right edge of the section, while a concentration of spirally flowing oil was observed in the bottom left-hand corner of the separator (Figure 14). For the presented New AAOS and C15RS2 geometries, the oil in the cylindrical section performs one full turn. For the New AAOS case, due to a decrease in  $D$ , the space between the cylindrical part and the vortex finder was reduced (Figure 12).

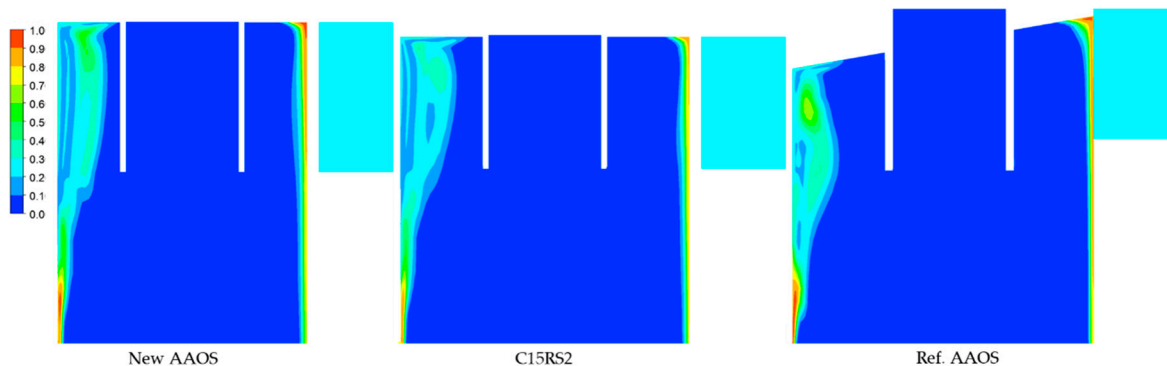


Figure 12. Average oil fraction contours—plane 1–1.

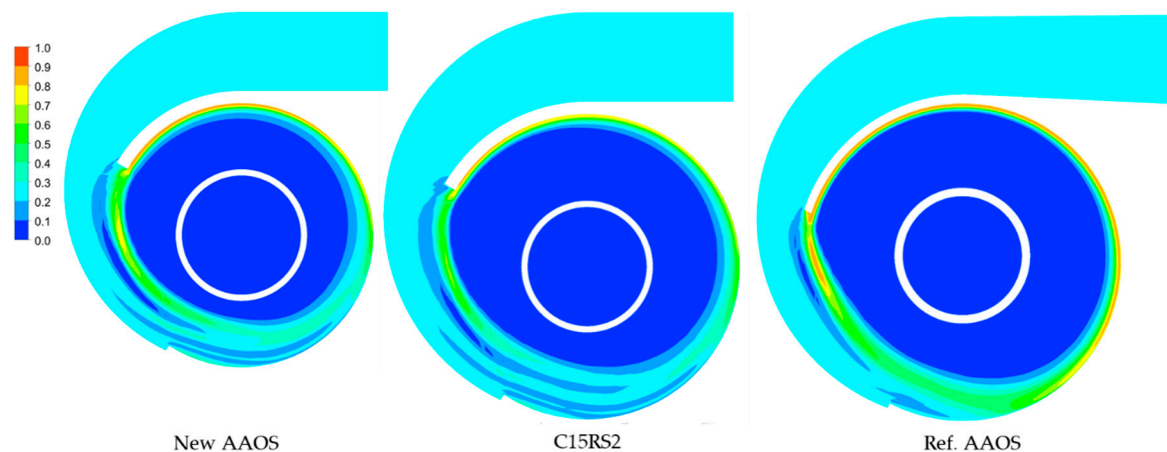
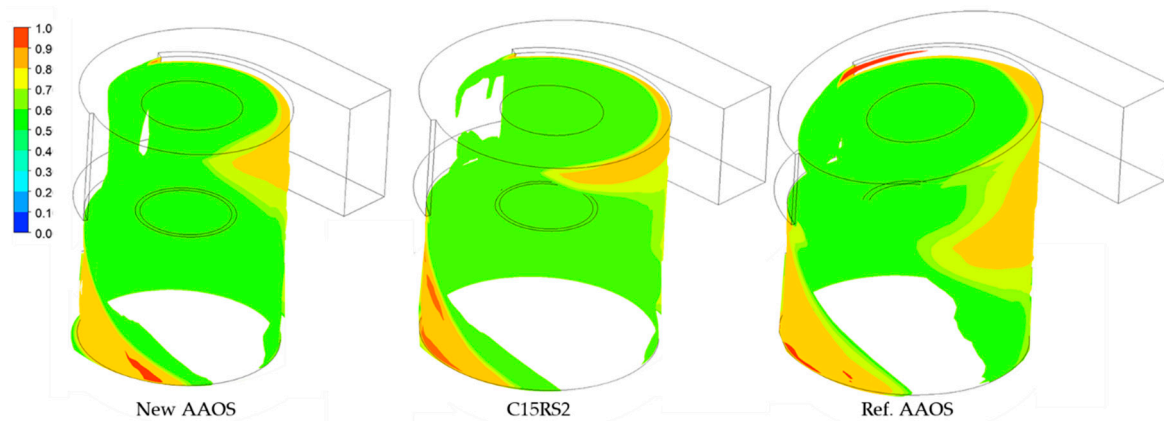


Figure 13. Average oil fraction contours.



**Figure 14.** Oil fraction 0.65, 0.8, 1 iso surface.

### 5.3.2. Velocity Contours

Figure 15 presents a comparison between tangential and axial velocity values related to the averaged inlet velocity of the New AAOS. Figure 2 includes lines L and K which mark the intersections of the two planes for which velocities were analysed. For the Ref. AAOS, there is an inclined inlet channel, which is narrowed in two dimensions—height and width. This results in the mixture acceleration and higher tangential and axial velocities at the separator inlet compared to the New AAOS and C15RS2 configurations (Figure 15A,B). Analysing the distribution on line L, the tangential velocity of the Ref. AAOS was higher by 0.9 compared to the others. The tangential velocity values in the central part of the separator do not differ from each other significantly (the maximum difference was 0.2), but in the boundary layer (near the wall), the differences are noticeable (Figure 15A,C). It can be seen that a change in diameter  $D$  does not involve significant changes in the tangential velocity profiles. However, a reduction in  $D$  increased the axial velocity for the New AAOS in the central part (range  $r/R = -0.6 - 0.6$ ) (Figure 15B,D).

In the central part of the separator ( $\pm 0.1 r/R$ ), the difference in velocity between the New AAOS and the Ref. AAOS is about 0.1. Near the wall in the inlet ( $-0.9 r/R$ ), the Ref. AAOS velocity is higher by about 0.3 compared to the New AAOS, while for the opposite wall, the C15RS2 and the New AOSA have almost the same velocities (Figure 15C). Below the vortex finder ( $\pm 0.2 r/R$ ), the axial velocity was by about 0.3 higher, and at the wall ( $\pm 0.9 r/R$ ) on both sides, the velocity of the Ref. AAOS was higher by about 0.3 compared to the New AAOS, which was due to the absence of oil in this region (Figure 15D). In both lines (L and K), the zero point of tangential velocity is in or close to the axis of the vortex finder. The axial velocity zero point locations are similar for the two lines under consideration and are as follows:  $-0.75 r/R$  for the left side and about  $0.8 r/R$  for the right side of the separator (Figure 15B,D).

Theoretically, the aim of increasing velocity in the separator is to improve efficiency and OQ by increasing the centrifugal force acting on the mixture; but in the case of the Ref. AAOS, it was noticed that a part of the stream of the mixture flowing from the inlet into the separator space was directed downwards to the separator outlet without making the spiral motion in the cylindrical part (Figure 14C). In the case of the New AAOS and the C15RS2 configuration, the inlet was not inclined, which lessened the impact on the velocity axial component below the inlet (Figure 15B,D). It was observed that too high an axial velocity could result in a low value of OQ due to the shortening of the distance covered by the mixture in the separator. Improper cooperation between the separator and the tank can also cause a decrease in the OQ value. A high velocity of the separated stream leaving the separator may have an unfavourable effect on the free surface of oil in the tank causing oil sloshing and, consequently, oil re-aeration.

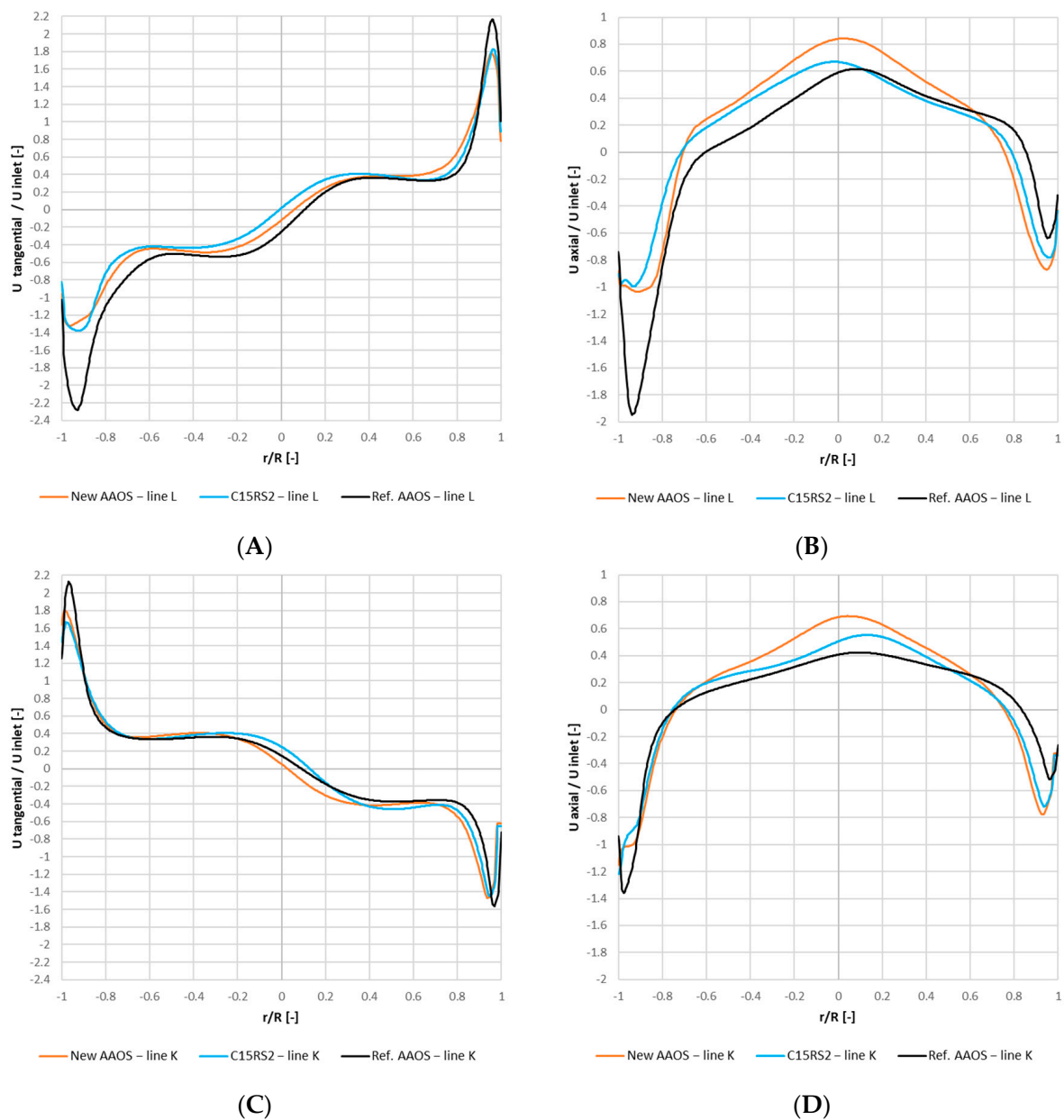


**Figure 15.** (A) tangential velocity at line L; (B) axial velocity at line L; (C) tangential velocity at line K; (D) axial velocity at line K.

The tangential velocity value for the Ref. AAOS is higher compared to the other geometries at the cylindrical part inlet and in the top part of the separator opposite the inlet. Higher velocities occur at the wall (for  $-0.9 r/R$ ), which is due to the smaller surface area of the inflow to the cylindrical part—it is smaller by 27% compared to the New AAOS case. For the horizontal inlet, the velocity distributions are similar. In all the geometries, the highest tangential velocity occurred close to the inlet channel (Figure 16).

Figure 17 presents the contour of the axial velocity on Plane 1–1. For the New AAOS and the C15RS2 configurations, the flow field below the vortex finder shows symmetry of the axial velocity compared to the Ref. AAOS (Figure 15B,D). This is another effect of the structure of the inlet and of the inclination of the separator upper plane.

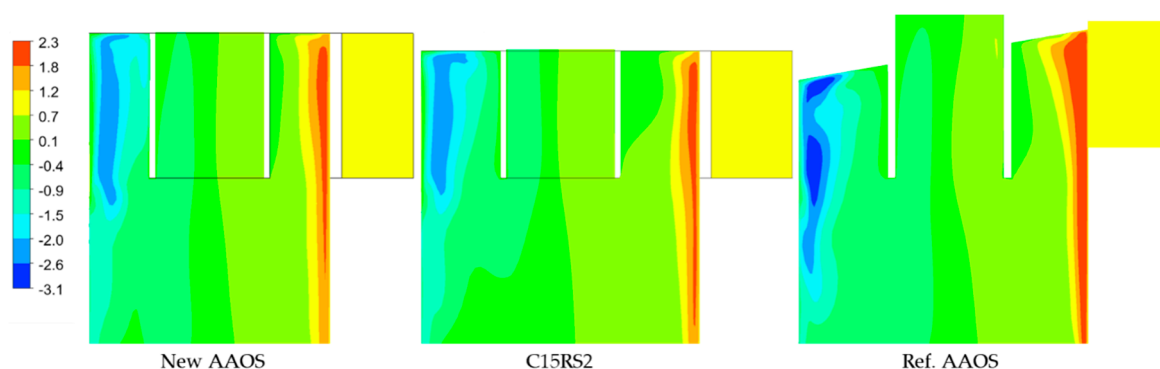


Figure 16. Time-averaged tangential velocity—plane 1–1.

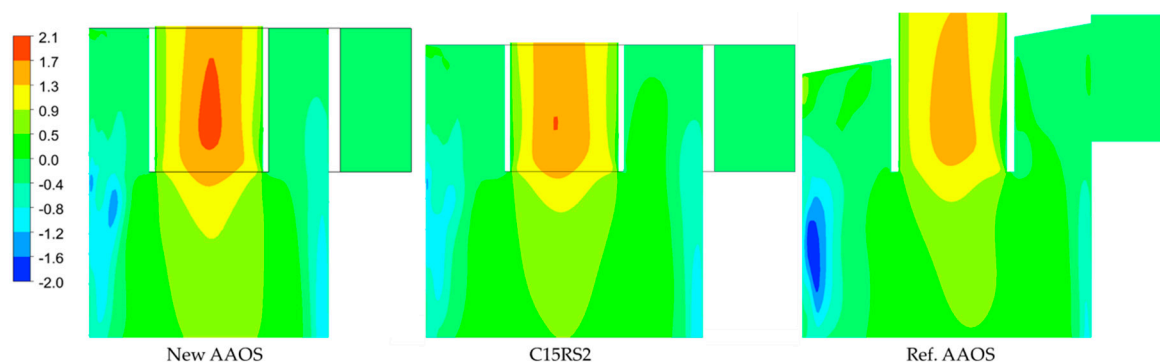


Figure 17. Time-averaged axial velocity—plane 1–1.

## 6. Summary and Conclusions

An analysis using the Fluent and the DesignXplorer software was conducted to determine the relations between the AAOS performance parameters ( $OQ$ , efficiency and  $dP$ ) and the separator geometric dimensions. The analysis was based on the results of CFD numerical simulations using the VOF fluid model and the RNG  $k - \epsilon$  turbulence model, the assumptions of which were verified previously by our own research based on experimental results [9,11]. The impact of 3 out of 6 geometric parameters was investigated ( $a$ ,  $b$ ,  $D$ ) using two ranges of the  $b/a$  ratio. The selection of the parameters was preceded by an analysis of the literature, and geometrical limitations were taken into account. Pareto analysis was performed to define the impact of geometric parameters on the separator performance. The Response Surface Method with the non-parametric regression algorithm was selected, and optimisation was carried out using the genetic algorithm. A comparison of the CFD results was made between the new and the reference geometry.

The following conclusions were drawn from the analysis:

- the applied CFD model enables simulations of the flow in the aircraft cyclone separator to analyse the impact of geometric parameters on the device performance,
- the Pareto analysis results indicate that in the ranges under consideration geometric parameters  $a$  and  $b$ , unlike diameter  $D$ , have a significant effect on the separator performance,
- the RSM indicated the  $b/a$  and the  $h/D$  ratios for which the AAOS operating parameters are the best,
- the comparison of the results of the CFD simulations for the New AAOS and the Ref. AAOS points to a difference in the formation of the oil film and a reduction in the velocity components at the separator wall, which translates into a higher  $OQ$  value and a lower pressure drop for the New AAOS variant,
- the obtained ratios of the separator dimensions differ from the Stairmand ratios; the separator inlet is higher and narrower,
- the Ref. AAOS reached a 26% lower relative value of  $OQ$  and a 50% higher pressure drop compared to the New AAOS,

- it is important to direct the mixture stream properly so that it should perform as many full turns in the cylindrical part as possible.

The possible further research should be extended by:

- investigations of the impact of the vortex finder geometry ( $D_x$ ,  $S$ ) and of the height of the separator cylindrical part below the inlet ( $h - b$ ); the studies should also concern the effect of the separator inlet inclination,
- investigations of the impact of additional geometric features to avoid the mixing of separated oil with the stream of the inlet mixture,
- numerical analysis of the oil level in the separator,
- experimental testing of the new separator geometry.

**Author Contributions:** Conceptualization, T.S., W.W. and T.B.; Data curation, T.S.; Formal analysis, T.S. and W.W.; Investigation, T.S.; Methodology, T.S.; Software, T.S.; Supervision, W.W. and T.B.; Validation, W.W.; Visualization, T.S.; Writing—original draft, T.S. and W.W. All authors have read and agreed to the published version of the manuscript.

**Funding:** This research received no external funding.

**Acknowledgments:** Publication supported under the rector's pro-quality grant for W.Wróblewski. Silesian University of Technology, grant number 08/050/RGJ22/00263.

**Conflicts of Interest:** The authors declare no conflict of interest.

## References

1. Barth, W. Design and layout of the cyclone separator on the basis of new investigations. *Brennstow-Wärme-Kraft* **1956**, *8*, 1–9.
2. Hoffmann, A.C.; Stein, L.E. *Gas Cyclones and Swirl Tubes*; Springer: Berlin/Heidelberg, Germany, 2008.
3. Stairmand, C.J. Pressure drops in cyclone separators. *Ind. Eng. Chem.* **1949**, *16*, 409–411.
4. Iozia, D.L.; Leith, D. The Logistic Function and Cyclone Fractional Efficiency. *Aerosol Sci. Technol.* **1990**, *12*, 598–606. [[CrossRef](#)]
5. Ramachandran, G.; Leith, D.; Dirgo, J.; Feldman, H. Cyclone Optimization Based on a New Empirical Model for Pressure Drop. *Aerosol Sci. Technol.* **1991**, *15*, 135–148. [[CrossRef](#)]
6. Casal, J.; Martinez-Benet, J.M. A better way to calculate cyclone pressure drop. *Chem. Eng.* **1983**, *90*, 99–100.
7. Shepherd, C.B.; Lapple, C.E. Flow Pattern and Pressure Drop in Cyclone Dust Collectors Cyclone without Intel Vane. *Ind. Eng. Chem.* **1940**, *32*, 1246–1248. [[CrossRef](#)]
8. Tauber, T.; D'Ambrosia, S.; Rudbarg, F. A lube system diagnostic monitor with deaeration capability. In *Turbo Expo: Power for Land, Sea, and Air, Proceedings of the ASME 1982 International Gas Turbine Conference and Exhibit, London, UK, 18–22 April 1982*; American Society of Mechanical Engineers: New York, NY, USA, 1982; pp. 1–6. [[CrossRef](#)]
9. Szwarc, T.; Wróblewski, W.; Borzęcki, T. Analysis of a cylindrical cyclone separator used in aircraft turbine engine. *Tech. Sci.* **2020**, *23*, 131–142. [[CrossRef](#)]
10. Furino, S. *Parametric Analysis of the Deaerator Flow Field Using CFD*; Politecnico di Torino: Torino, Italy, 2020.
11. Szwarc, T.; Wróblewski, W.; Borzęcki, T. Experimental and numerical study of the impact of the oil tank filling level on the aircraft separator. In *Facta Universitatis, Series: Mechanical Engineering*; University of Niš: Niš, Serbia, 2022. [[CrossRef](#)]
12. Stairmand, C.J. The design and performance of cyclone separators. *Ind. Eng. Chem.* **1951**, *29*, 356–383.
13. Zhu, Y.; Lee, K.W. Experimental study on small cyclones operating at high flowrates. *J. Aerosol Sci.* **1999**, *30*, 1303–1315. [[CrossRef](#)]
14. Elsayed, K.; Lacor, C. The effect of cyclone inlet dimensions on the flow pattern and performance. *Appl. Math. Model.* **2011**, *35*, 1952–1968. [[CrossRef](#)]
15. Gao, Z.; Wang, J.; Liu, Z.; Wei, Y.; Wang, J.; Mao, Y. Effects of different inlet structures on the flow field of cyclone separators. *Powder Technol.* **2020**, *372*, 519–531. [[CrossRef](#)]
16. Elsayed, K.; Lacor, C. Numerical modeling of the flow field and performance in cyclones of different cone-tip diameters. *Comput. Fluids* **2011**, *51*, 48–59. [[CrossRef](#)]
17. Elsayed, K.; Lacor, C. Modeling and Pareto optimization of gas cyclone separator performance using RBF type artificial neural networks and genetic algorithms. *Powder Technol.* **2012**, *217*, 84–99. [[CrossRef](#)]
18. Kha, H.M.; Phuong, N.N.; Nam, N.T. The Effect of Different Geometrical Configurations of the Performances of Gas-Liquid Cylindrical Cyclone Separators (GLCC). In *Proceedings of the 2017 International Conference on System Science and Engineering (ICSSE), Ho Chi Minh City, Vietnam, 21–23 July 2017*; pp. 646–651.
19. Erdal, F.M.; Shirazi, S.A.; Shoham, O.; Kouba, G.E. CFD simulation of single-phase and two-phase flow in Gas-Liquid Cylindrical Cyclone separators. *SPE J.* **1997**, *2*, 436–445. [[CrossRef](#)]

20. Erdal, F.M.; Shirazi, S.A.; Mantilla, I.; Shoham, O. CFD study of bubble carry-under in gas-liquid Cylindrical Cyclone separators. In Proceedings of the SPE Annual Technical Conference and Exhibition, New Orleans, LO, USA, 27–30 September 1998; Volume 1999, pp. 781–791. [[CrossRef](#)]
21. Brar, L.S.; Sharma, R.P. Effect of varying diameter on the performance of industrial scale gas cyclone dust separators. *Mater. Today Proc.* **2015**, *2*, 3230–3237. [[CrossRef](#)]
22. Elsayed, K. Analysis and Optimization of Cyclone Separators Geometry Using RANS and LES Methodologies Khairy Elsayed. In *Turbulence and Interactions*; Springer: Berlin/Heidelberg, Germany, 2011; pp. 65–74.
23. Elsayed, K.; Lacor, C. Optimization of the cyclone separator geometry for minimum pressure drop using mathematical models and CFD simulations. *Chem. Eng. Sci.* **2010**, *65*, 6048–6058. [[CrossRef](#)]
24. Elsayed, K.; Lacor, C. CFD modeling and multi-objective optimization of cyclone geometry using desirability function, Artificial neural networks and genetic algorithms. *Appl. Math. Model.* **2013**, *37*, 5680–5704. [[CrossRef](#)]
25. Singh, P.; Couckuyt, I.; Elsayed, K.; Deschrijver, D.; Dhaene, T. Shape optimization of a cyclone separator using multi-objective surrogate-based optimization. *Appl. Math. Model.* **2016**, *40*, 4248–4259. [[CrossRef](#)]
26. Sun, X. Multi-objective optimization of a Stairmand cyclone separator using response surface methodology and computational fluid dynamics. *Powder Technol.* **2017**, *320*, 51–65. [[CrossRef](#)]
27. Sun, X.; Yoon, J.Y. Multi-objective optimization of a gas cyclone separator using genetic algorithm and computational fluid dynamics. *Powder Technol.* **2018**, *325*, 347–360. [[CrossRef](#)]
28. Hirt, C.W.; Nichols, B.D. Volume of fluid (VOF) method for the dynamics of free boundaries. *J. Comput. Phys.* **1981**, *39*, 201–225. [[CrossRef](#)]
29. Yakhot, V.; Orszag, S.A. Renormalization group analysis of turbulence. *I. Basic theory. J. Sci. Comput.* **1986**, *1*, 3–51. [[CrossRef](#)] [[PubMed](#)]
30. Box, G.E.P.; Draper, N.R. *Empirical Model Building and Response Surfaces*; John Wiley and Sons: New York, NY, USA, 1987.
31. Ravi, G.; Gupta, S.K.; Ray, M.B. Multiobjective optimization of cyclone separators using genetic algorithm. *Ind. Eng. Chem. Res.* **2000**, *39*, 4272–4286. [[CrossRef](#)]
32. Sgrott, O.L.; Noriler, D.; Wiggers, V.R.; Meier, H.F. Cyclone optimization by COMPLEX method and CFD simulation. *Powder Technol.* **2015**, *277*, 11–21. [[CrossRef](#)]